



An electrochemical peptide-based biosensor for the Alzheimer biomarker amyloid- $\beta_{(1-42)}$ using a microporous gold nanostructure

Masoud Negahdary¹ · Hossein Heli¹

Received: 1 June 2019 / Accepted: 6 October 2019 / Published online: 12 November 2019
© Springer-Verlag GmbH Austria, part of Springer Nature 2019

Abstract

Alzheimer's disease (AD) is connected to aggregation of amyloid- β ($A\beta$) peptide and formation of insoluble plaques in the brain. $A\beta$ level can be monitored as an AD early diagnosis route. In this study, an irregular shaped microporous gold nanostructure with a typical size of 150×250 nm was electrodeposited on a polycrystalline gold surface at 0 mV (vs. AgCl) using sodium alendronate. The nanostructure was then characterized by field-emission scanning electron microscopy. An electrochemical peptide-based biosensor was fabricated by immobilizing an $A\beta_{(1-42)}$ -binding peptide on the gold nanostructure. Binding of $A\beta_{(1-42)}$ by the peptide was followed electrochemically using ferro/ferricyanide as a redox probe. Differential pulse voltammograms in a potential range of 0–500 mV (vs. AgCl) with typical peak potentials at 224 mV are linear in the 3–7000 pg mL^{-1} $A\beta_{(1-42)}$ concentration range, with a 0.2 pg mL^{-1} detection limit. The biosensor is free of interferences and was applied to the quantitation of $A\beta_{(1-42)}$ in artificial cerebrospinal fluid and spiked serum samples.

Keywords β -Amyloid $_{(1-42)}$ · Peptisensor · Beta-amyloid · Neurodegenerative disease · Pathophysiology · Nanoparticles · Blood · Clinical diagnosis

Introduction

Alzheimer's disease (AD) is related to aggregation of amyloid- β ($A\beta$) as β -sheet conformation and formation of insoluble plaques in the brain [1]. $A\beta_{(1-40)}$ and $A\beta_{(1-42)}$ are well-known forms of this oligopeptide. $A\beta_{(1-42)}$ has a higher tendency toward aggregate and neuronal cell death. $A\beta$ level can be monitored in biofluids such as cerebrospinal fluid (CSF), whole blood, plasma and serum as AD early diagnosis before incidence symptoms of dementia. In patients suffering from AD, the concentration of $A\beta$ in the CSF decreases due to accumulation in the brain (<500 pg mL^{-1}) [2], and accumulated $A\beta$ fibrils can be released in the bloodstream. So far, various methods were reported for early diagnosis of AD including enzyme-linked immunosorbent assay (ELISA) [3],

electrochemiluminescence [4], surface-enhanced Raman spectroscopy [5], electroanalysis [6], fluorometry [7], localized surface plasmon resonance [8], and ultraviolet-visible spectrophotometry [9]. False-negative diagnoses, high cost, time consuming operation, feeble sensitivity, and low stability are some of disadvantages of these assays. Finding highly sensitive, selective and stable diagnosis methods to $A\beta$ determination is essential and required.

Antibodies, aptamers, peptides and artificial receptors have been used extensively as biorecognition elements in biosensors fabrication [10–12]. The goal of diversity in the biorecognition element is usually to improve the sensitivity and specificity of the biosensors. However, antibodies suffer from some important disadvantages such as expensive production, inability to cause chemical modification, and irreversible thermal denaturation [13]. Although aptamers have important benefits including high stability, quick chemical production, none-immunogenicity, flexible conformation and easy chemical modification [14], there are several limitations such as nuclease degradability, tertiary structure dependence on the solution characters, renal filtration in some in-vivo applications, and interaction with some intracellular and similar-structure targets [15]. Synthetic peptides have some major advantages including easy C-terminus modification, small size, being chemically defined and none-immunogenicity [16].

Electronic supplementary material The online version of this article (<https://doi.org/10.1007/s00604-019-3903-x>) contains supplementary material, which is available to authorized users.

✉ Hossein Heli
hheli7@yahoo.com; heli@sums.ac.ir

¹ Nanomedicine and Nanobiology Research Center, Shiraz University of Medical Sciences, Shiraz 7193635899, Iran

The use of nanostructures in the design of biosensors has led to an increase in the surface concentration of the biorecognition element, creation of a specific location for the optimal immobilization of the biorecognition element, increment in binding the target into the immobilized biorecognition element and improvement in the electron transfer process [10, 11]. For preparation of a suitable nanostructured transducer surface via electrodeposition, the components of synthesis solution and electrodeposition conditions are important and effective, and should be controlled [17]. Gold nanostructures are multifunctional, conjugatable and morphologically tunable, and have specific localized surface plasmon resonance properties, controllable surface chemistry, a high surface-to-volume ratio, and high biocompatibility leading to a variety of applications in different areas including diagnostics, sensing, imaging, and therapy [18–20].

In this study, a specific peptide sequence creates a strong and successful bond with the surface of a microporous gold nanostructure through the thiol group of its cysteine residue to fabricate an $A\beta_{(1-42)}$ biosensor. In designing and selecting this peptide sequence, a high specificity to capture $A\beta_{(1-42)}$ was considered. For electrodeposition of the microporous gold nanostructure, alendronate was employed as an amine-bearing molecule and shape directing agent to attain a special morphology and uniform surface. Ferrocyanide/ferricyanide redox couple was employed as a redox marker to quantify $A\beta_{(1-42)}$ in clinical samples.

Materials and methods

Reagents and chemicals

$A\beta_{(1-42)}$, heparin, hemoglobin, human serum albumin (HSA), bilirubin, tetrachloroauric acid, alendronate sodium, potassium chloride, potassium ferricyanide and potassium ferrocyanide were purchased from Sigma (USA, sigmaaldrich.com). 6-Mercapto-1-hexanol (MCH), ethyl acetate, dithiothreitol (DTT), sulfuric acid, hydrochloric acid and hydrogen peroxide were purchased from Scharlau (Spain, scharlab.com). Deionized water (DW) was employed to prepare the solutions. A specific peptide sequence of CPPPPTHSSQWLNKPSKPKTNMK was purchased from PepTron (Korea, peptron.com).

Apparatus

The microporous gold nanostructure was evaluated by field-emission scanning electron microscopy (FESEM) with energy-dispersive X-ray spectroscopy (EDS) capability, using a TESCAN Mira 3-XMU microscope (Czech Republic, tescan.com).

A digital voltmeter of Mastech MS8340B (China, mastech-group.com) was used to measure the open circuit potential

(OCP) of the working electrode during immobilization of the peptide. Voltammetric studies were performed using a potentiostat/galvanostat of μ -Autolab (the Netherlands, metrohm-autolab.com) equipped with the GPES software. A conventional three-electrode system comprising a gold disk (Au) electrode of 2 mm in diameter as the working, a platinum wire as the counter, and a silver/silver chloride, 3 mol L⁻¹ potassium chloride as the reference electrode were employed. Differential pulse voltammograms (DPVs) at a pulse time of 50 ms, a potential sweep rate of 10 mV s⁻¹ and a pulse width of 25 mV were recorded. All measurements were performed at room temperature otherwise stated.

Synthesis of microporous gold nanostructure

Firstly, the Au electrode (of 2 mm in diameter) was polished on a polishing pad and then on 0.05- μ m alumina powder until a mirror-like surface was observed. Then, the electrode was rinsed with DW and then immersed in a 3:1 ethanol/water mixture and sonicated in an ultrasound bath for 8 min. The Au electrode was dipped in a solution containing 20 mmol L⁻¹ tetrachloroauric acid, 500 mmol L⁻¹ sulfuric acid and 150 mmol L⁻¹ sodium alendronate. Electrodeposition was performed at 0 mV during 300 s and the resultant electrode was denoted as the MGN/Au electrode.

Fabrication and evaluation of the biosensor

The preformed S-S bond between the peptide molecules was broken by DTT. 50 μ L of 10 μ mol L⁻¹ peptide solution was mixed with 10 μ L 500 mmol L⁻¹ DTT for 20 min. Then, 100 μ L ethyl acetate was added and mixed by a vortex; then, the upper layer was discarded for three repeated times. 10 μ L of the resultant solution was immediately dropped on the surface of the MGN/Au electrode and leaved at 4 °C for a desired time. After that, the electrode was rinsed with DW, and 10 μ L 1 mmol L⁻¹ MCH was dropped on the electrode surface and leaved at room temperature for 30 min. After final rinsing with DW, the biosensor was attained.

To optimize the immobilization time of the peptide on the microporous gold nanostructure surface, we electrodeposited the working electrode of the screen printed electrodes from DropSens (Spain, dropsens.com) followed by dropping the peptide, while OCP changes were measured over time at 4 °C.

To find the optimized time of binding of $A\beta_{(1-42)}$ into the immobilized peptide (the biosensor surface), we bound 100 pg mL⁻¹ $A\beta_{(1-42)}$ at each 5-min interval at 37 °C, transferred the biosensor into a 20 mmol L⁻¹ tris(hydroxymethyl)aminomethane hydrochloride solution, pH = 7.4 (Tris buffer) containing 0.5 mol L⁻¹ potassium chloride and 0.5 mmol L⁻¹ ferrocyanide/ferricyanide (1:1), and DPVs were measured at each binding time. This experiment

(prolonging the binding time) was continued till the peak current in DPVs reached a constant value.

To quantify $A\beta_{(1-42)}$ using the biosensor, we captured different concentrations of $A\beta_{(1-42)}$ (0.003, 0.01, 0.03, 0.1, 0.3, 0.5, 1, 3, 5 and 7 ng mL^{-1}) dissolved in Tris buffer by the biosensor and measured DPVs for each concentration.

Analysis of real samples

50 mL artificial CSF was prepared by mixing desired amounts of the following materials to attained the reported concentrations. Artificial CSF contained potassium chloride of 2.5 mmol L^{-1} , magnesium chloride of 1.2 mmol L^{-1} , D-glucose of 10 mmol L^{-1} , calcium chloride of 2.0 mmol L^{-1} , sodium dihydrogen phosphate of 1.24 mmol L^{-1} , sodium chloride of 126 mmol L^{-1} and sodium hydrogen carbonate of 26 mmol L^{-1} , that adjusted at $\text{pH} = 7.35$ (by adding HCl or NaOH of 100 mmol L^{-1}) and bubbled with 95% air and 5% CO_2 . Serum samples (from 5-mL blood samples) were obtained from healthy individuals. Five serum and five CSF samples were diluted (final dilution ratio of 1:1) with Tris buffer containing 0.5 mol L^{-1} potassium chloride and 0.5 mmol L^{-1} ferrocyanide/ferricyanide (1:1), spiked with stock $A\beta_{(1-42)}$ solutions of 20, 50, 200 or 1000 pg mL^{-1} prepared in Tris buffer to attain different concentrations of $A\beta_{(1-42)}$ (2, 5, 20, 50 and 200 pg mL^{-1}). DPVs were measured for these spiked samples and analyzed similar to previous section.

Results and discussion

Choice of materials

Nanostructures of noble metals (especially gold) having diversity in shape, size and morphology are highly attracted because of unique physicochemical properties. Among the noble metals and nanostructures, anisotropic gold nanostructures represent high (re)activity and surface area making them suitable for fabrication of biosensors transducer. For synthesis of gold nanostructures, electrodeposition is a potentially interested route due to advantages of easy controllability, preparation of the nanostructures as pure and uniform deposits, and tenability for fabrication of a variety of zero to two dimension nanostructures [10, 11, 17]. Therefore, electrodeposition of a microporous gold nanostructure with a high surface area was followed in this study to immobilize a thiolated $A\beta_{(1-42)}$ -specific peptide with a high surface concentration. This led to amplification of the electrochemical signals arriving at increment in the detection sensitivity and specificity. As for the peptide, the last 16-amino acids row of the peptide sequence is specific to capture $A\beta_{(1-42)}$ [21]; the cysteine-terminal of the peptide acts as a linker to the surface of microporous gold nanostructure through the thiol (functional group of cysteine)-

gold binding, and the PPPP row acts as a spacer to place a distance between the capturing part and the transducer surface.

Characterization of the microporous gold nanostructure

In order to investigate surface morphology and structure of the microporous gold nanostructure, FESEM images at different magnifications were recorded, and are shown in Fig. 1a, b. The images show that the gold nanostructure comprising of irregular shaped objects covers the entire surface with typical size of 150×250 nm. These nanostructures provided a high porosity surface full of “micro”scale pinholes at the surface. The EDS spectrum shown in Fig. 1c also confirmed the purity of the microporous gold nanostructure without deposition/adsorption/occupation of sodium alendronate. As to the role of sodium alendronate in the electrodeposition of the microporous gold nanostructure, it should be noted that different additives with different functional groups affect the morphology, structure and size of electrodeposited gold structures [10, 11, 17, 18]. The applied potential led to a rapid formation of gold nuclei that was also accelerated by the underlying gold substrate [22]. Alendronate at once coordinated and formed partial electrostatic complex with these gold nuclei [23] through its primary amine group [24] on the (1 1 1) gold plane surface. Further growth was then followed along this (1 1 1) direction.

To check the privilege of the microporous gold nanostructure to use as the biosensor transducer, we electrochemically determined the true surface area of the MGN/Au electrode (and the Au electrode as well) using the redox transition of ferrocyanide/ferricyanide (1:1, 0.5 mmol L^{-1}) in 0.5 mol L^{-1} KCl and 20 mmol L^{-1} tris(hydroxymethyl)aminomethane hydrochloride, $\text{pH} = 7.4$ by recording cyclic voltammograms at different potential sweep rates. Supplementary material S1 demonstrates these voltammograms and the corresponding analysis. According to these results, the true surface area of the MGN/Au and Au electrodes was obtained as 0.185 and 0.032 cm^{-2} , respectively, indicating a roughness factor of 5.7 (compared to the true surface area of the Au electrode) or 5.9 (compared to the geometric surface area of the Au electrode) for the MGN/Au electrode. As indicated above, and as expected, the microporous gold nanostructure can provide a high peptide surface concentration.

Fabrication of the biosensor and quantitation of $A\beta_{(1-42)}$

To prepare the biosensor through immobilization of the peptide on the MGN/Au electrode surface, the time of peptide-microporous gold nanostructure incubation should be optimized. Changes in the OCP value of the MGN/Au electrode during immobilization of the peptide are shown in Supplementary material S2. For the peptide, values of the

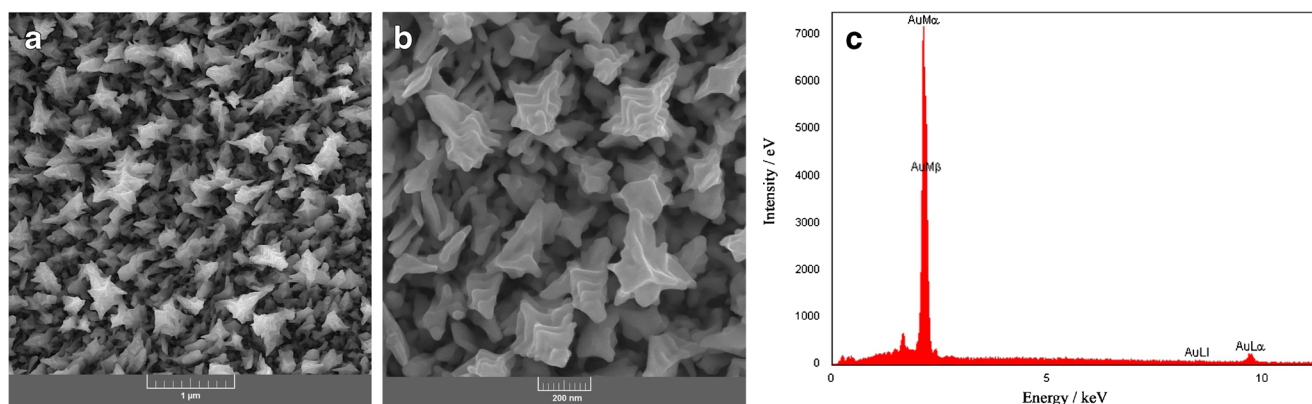
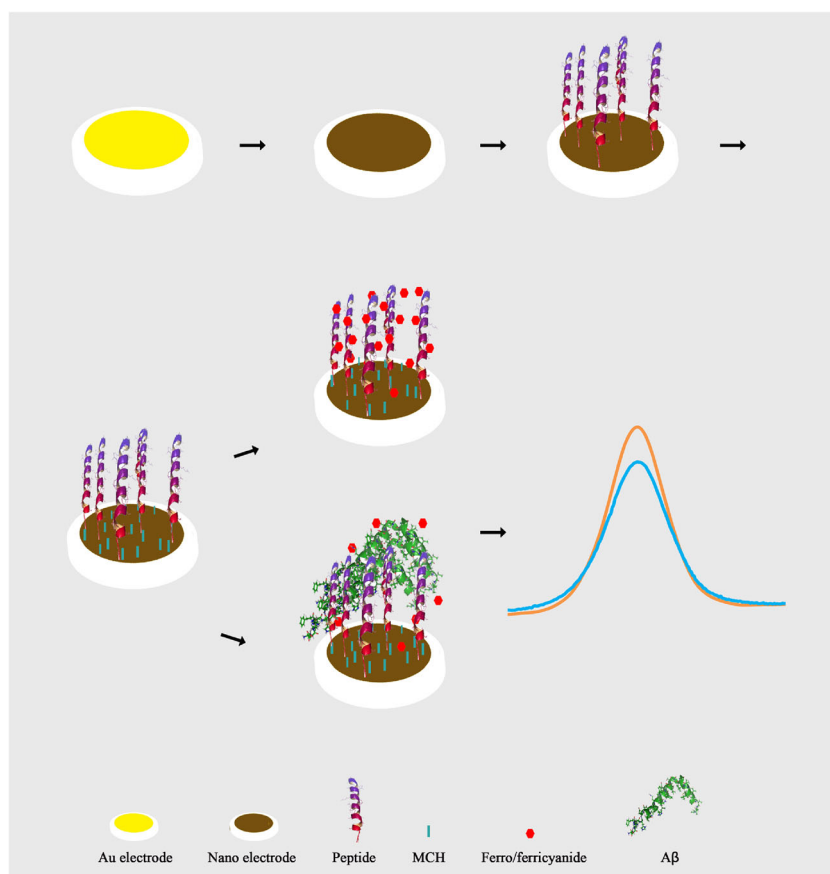


Fig. 1 **a, b** FESEM images of the microporous gold nanostructure at different magnifications. **c** an EDS spectrum of the nanostructure

point of isoelectric of 9.24 [25], 10.78 [26] and 10.81 [27] can be calculated. In any case, the peptide had a net positive charge at physiological pH (working pH of the biosensor), and its immobilization progression led to decrement in the negative potential; it and reached the stable value after about 80 min. This time that was selected for the peptide immobilization was shorter than that reported for the immobilization of thiolated oligonucleotide on some different gold nanostructures [10] and a thiolated aptamer on an array of gold nanodumbbells [11].

Supplementary material S3 shows DPVs recorded using the biosensor after binding 0.1 ng mL^{-1} $\text{A}\beta_{(1-42)}$ at different times. Upon increment in the binding time, the peak current lowered and after 30 min reached a stable value and remained constant upon prolonging the binding time. Therefore, 30 min was selected as the optimized binding time. This time is shorter than the optimized binding time of thrombin-antibody and thrombin-aptamer [28], platelet-derived growth factor-aptamer [29], thrombin-aptamer [30] prostate-specific antigen-aptamer [31], and troponin I-aptamer [11]. Before

Scheme 1 The biosensor fabrication procedure and $\text{A}\beta_{(1-42)}$ determination



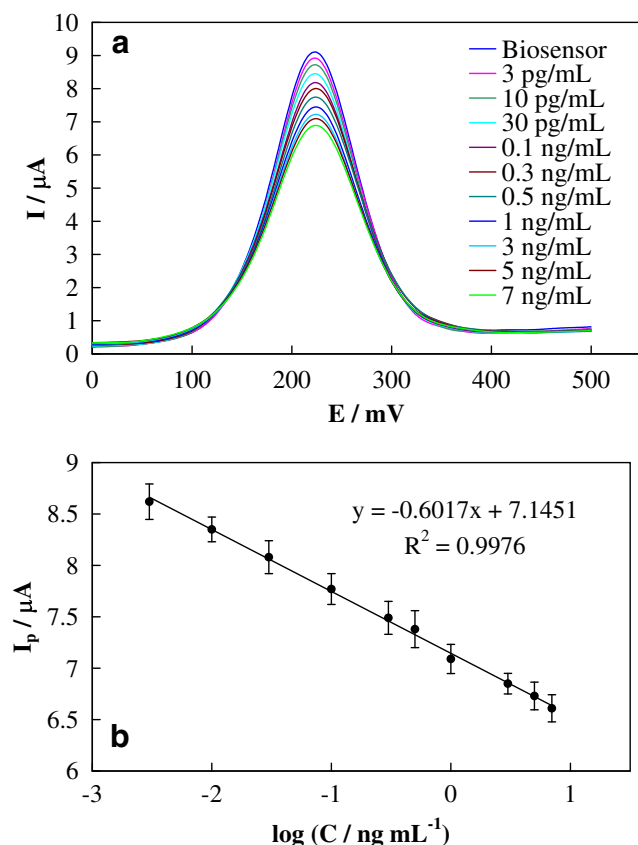


Fig. 2 **a** DPVs recorded using the biosensor before and after capturing $A\beta_{(1-42)}$ of different concentrations of 0, 0.003, 0.01, 0.03, 0.1, 0.3, 0.5, 1, 3, 5 and 7 ng mL^{-1} . **b** Dependency of the peak currents on the $A\beta_{(1-42)}$ concentration derived from panel (a) as a calibration plot. The peak currents were measured at 224 mV

capturing $A\beta_{(1-42)}$, the biosensor surface had a specific positive surface charge related to protonation of the peptide amino acids, and the redox marker had a desired access to the biosensor surface for electron exchange. The redox marker signal is, therefore, high due to electrostatic attraction of the marker and the biosensor surface; usually, the biorecognition elements bear negative charge at physiological pH. Upon $A\beta_{(1-42)}$ binding, the negative surface charge of the biosensor was increased because $A\beta_{(1-42)}$ has an isoelectric point of 5.31 [32], and in the working pH of the biosensor, it has a net negative charge. The biosensor fabrication procedure and $A\beta_{(1-42)}$ determination are schematically presented in Scheme 1.

Table 1 Precision ($n = 3$) for assay of three $A\beta_{(1-42)}$ concentrations by the biosensor

$A\beta_{(1-42)}$ level / pg mL^{-1}	RSD% (intra-day assay)	RSD (inter-day assay)
10	3.79	5.35
30	2.08	5.17
200	3.15	3.79

Figure 2a shows DPVs recorded using the biosensor before and after capturing $A\beta_{(1-42)}$ of different concentrations of 0.003 to 7 ng mL^{-1} , and dependency of the peak current on the $A\beta_{(1-42)}$ concentration as a calibration plot is displayed in Fig. 2b. $A\beta_{(1-42)}$ concentration increment led to a regular decrement in the peak current due to repelling the redox marker from the biosensor surface after $A\beta_{(1-42)}$ binding. According the calibration plot, the regression equation is $I_p (\mu\text{A}) = (-0.6017 \pm 0.0104) \log (C_{A\beta_{(1-42)}}/\text{ng mL}^{-1}) + (7.1451 \pm 0.0129)$, $R^2 = 0.9976$. Considering a signal decrement value equal to $3 \times \text{SD}$ (where SD is the standard deviation of the blank signal) as the signal of the limit of detection (LOD) and the use of the slope of the calibration plot, LOD was obtained as 0.2 pg mL^{-1} .

Determination of $A\beta_{(1-42)}$ in plasma and CSF

In Alzheimer's disease, $A\beta_{(1-42)}$ plasma and CSF levels are lowered [33–35] because of aggregation in the brain [35]. Results of a study indicated $A\beta_{(1-42)}$ plasma levels as 18.05 ± 5.1 and $27.11 \pm 2.45 \text{ pg mL}^{-1}$ for Alzheimer's disease and elderly normal controls, respectively [34]. A cohort study was performed on normal subjects in three age ranges of ≤ 34 , $35 \leq \text{age} \leq 64$, and > 64 years [33]. The results showed that the normal plasma level of $A\beta_{(1-42)}$ had an average value of $17.65 \pm 5.71 \text{ pg mL}^{-1}$. In addition, $A\beta_{(1-42)}$ levels in CSF of healthy persons and Alzheimer's patients were obtained as 1678 ± 436 and $709 \pm 304 \text{ pg mL}^{-1}$, respectively [35]. Therefore, all of these $A\beta_{(1-42)}$ levels can be placed within the linear range of the biosensor, and the biosensor can determine the $A\beta_{(1-42)}$ levels as low as those reported for the biological fluids of the Alzheimer's patients. To compare the figure of the merit of the biosensor with those reported for other methods of $A\beta_{(1-42)}$ determination, a literature survey was performed and the result is presented in Supplementary material S4. This comparison indicated that the biosensor can detect a very low concentration of $A\beta$. Additionally, the reported methods were mainly immunosensing; the peptide-based biosensing had advantages such as high affinity of the peptide, simplicity over the antibody, lower cost, and resistance to immunogenicity.

Reproducibility and repeatability of the biosensor

In order to evaluate the reproducibility and repeatability of the biosensor, $A\beta_{(1-42)}$ solutions of three different concentrations were quantified through independent measurements over a same day (for intra-day assay) as well as three different days (for inter-day assay); the results are given in Table 1. In addition, an $A\beta_{(1-42)}$ solution of 0.1 ng mL^{-1} was quantified three times using one biosensor. A relative standard deviation (RSD) of 2.95% was attained.

Fabrication reproducibility of the biosensor was evaluated by 6 times fabrication of similar biosensors and after each

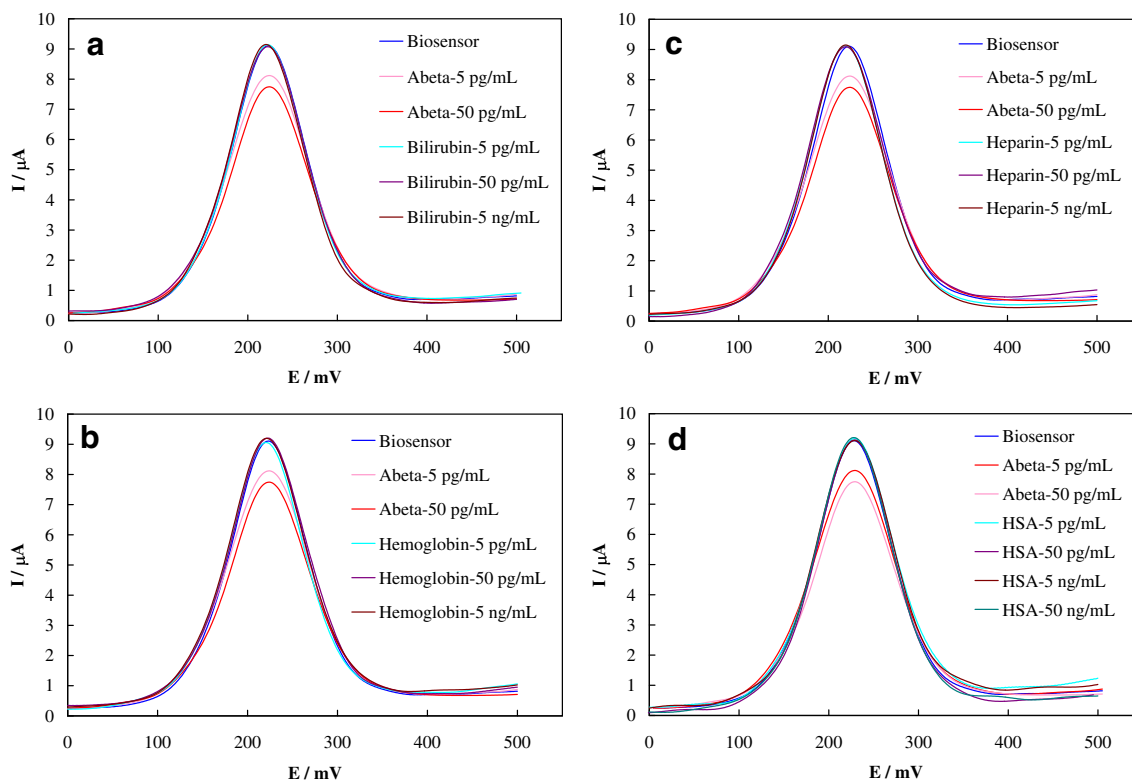


Fig. 3 DPVs recorded using the biosensor in the presence of **a** bilirubin, **b** hemoglobin, **c** heparin and **d** HSA at different concentrations

fabrication time, a DPV was recorded. The data are presented in Supplementary material S5. The peak current change in the voltammograms had a RSD value of 1.33%, indicating the reproducibility of the fabrication procedure.

To inspect the ability of the biosensor for re-analysis of a sample or multiple uses for analysis of several samples, we recorded a DPV using the biosensor. Then, it was bound with an $A\beta_{(1-42)}$ solution of 0.1 ng mL^{-1} and a DPV was measured. The biosensor was then dipped into hot DW at $90 \text{ }^\circ\text{C}$ for 5 min to release the bound $A\beta_{(1-42)}$. The biosensor was then rinsed with Tris buffer, and a DPV was recorded, rinsed with Tris buffer, and re-bound with the same $A\beta_{(1-42)}$ solution. This cycle was repeated five times, and the two five-set of DPVs are shown in Supplementary material S6. Change in the peak current difference before and after binding with $A\beta_{(1-42)}$ had a RSD value of 3.76%, indicating the good regeneration ability of the biosensor.

Stability, selectivity and applicability of the biosensor

The biosensor stability was determined by recording DPVs after binding with an $A\beta_{(1-42)}$ solution of 0.1 ng mL^{-1} in consecutive days. During this analysis, the biosensor was stored in Tris buffer at $4 \text{ }^\circ\text{C}$. Changes in the peak current over time are displayed in Supplementary material S7. It was observed that the peak current was decreased to 86% of its initial value after 14 days, and 70% after 17 days.

Selectivity of the biosensor was appraised by recording DPVs for binding different concentrations of bilirubin, hemoglobin, heparin and HAS, and are shown in Fig. 3. Values of the peak currents in these voltammograms are reported in Supplementary material S8. It should be noted that due to the high level of HSA in the serum, a higher concentration of 50 ng mL^{-1} was also checked. The results indicated that these interfering species did

Table 2 Determination of $A\beta_{(1-42)}$ in serum and artificial CSF samples by the biosensor

Sample	CSF#1	CSF#2	CSF#3	CSF#4	CSF#5	Serum#1	Serum#2	Serum#3	Serum#4	Serum#5
Amount added / pg mL^{-1}	2	5	20	50	200	2	5	20	50	200
Amount found / pg mL^{-1}	1.92	4.87	22	51	190	1.88	4.76	19.3	56	201
Percentage	96.0	97.4	110	102	95.0	94.0	95.2	96.5	112	100.5
RSD ($n = 3$)	6.5	4.0	2.8	3.9	1.6	1.5	4.5	1.1	3.3	4.0
Bias%	-4.0	-2.6	10	2.0	-5.0	-6.0	-4.8	-3.5	12	0.5

not significantly affect the biosensor signal with a very good selectivity.

To investigate the applicability of the biosensor in determination of $A\beta_{(1-42)}$ in real matrices, spiked serum and artificial CSF with $A\beta_{(1-42)}$ were quantified. The values added and obtained for $A\beta_{(1-42)}$ are displayed in Table 2. The values found by the biosensor and those added were in good accord confirming the applicability of the biosensor.

Conclusion

We used a simple electrodeposition procedure for preparation of a microporous gold nanostructure. The microporous nanostructure was checked for immobilization of an $A\beta_{(1-42)}$ specific peptide and detection of its binding with a high sensitivity. The high sensitivity would be due to favorable conformation of the immobilized peptide, deflection ability of the peptide for an efficient binding, higher peptide surface concentration, and/or enhanced diffusion regime of the marker. Simplicity, low-cost and lack of interference were other advantages of the biosensor. The biosensor would be applicable for point-of-care diagnosis of Alzheimer's disease.

Acknowledgments The financial support of the Iran National Science Foundation Grant NO. 96005985 is gratefully acknowledged. We would also like to thank the Research Councils of Shiraz University of Medical Sciences.

References

- Dubois B, Hampel H, Feldman HH, Scheltens P, Aisen P, Andrieu S, Bakardjian H, Benali H, Bertram L, Blennow K (2016) Preclinical Alzheimer's disease: definition, natural history, and diagnostic criteria. *Alzheimers Dement* 12(3):292–323
- Almdahl IS, Lauridsen C, Selnes P, Kalheim LF, Coello C, Gajdzik B, Moller I, Wettergreen M, Grambaite R, Bjornerud A, Brathen G, Sando SB, White LR, Fladby T (2017) Cerebrospinal fluid levels of amyloid beta 1-43 mirror 1-42 in relation to imaging biomarkers of Alzheimer's disease. *Front Aging Neurosci* 9:9. <https://doi.org/10.3389/fnagi.2017.00009>
- Englund H, Sehlin D, Johansson AS, Nilsson LN, Gellerfors P, Paulie S, Lannfelt L, Pettersson FE (2007) Sensitive ELISA detection of amyloid- β protofibrils in biological samples. *J Neurochem* 103(1):334–345
- Song X, Li X, Wei D, Feng R, Yan T, Wang Y, Ren X, Du B, Ma H, Wei Q (2019) CuS as co-reaction accelerator in PTCA-K2S2O8 system for enhancing electrochemiluminescence behavior of PTCA and its application in detection of amyloid- β protein. *Biosens Bioelectron* 126:222–229. <https://doi.org/10.1016/j.bios.2018.10.068>
- Yu X, Hayden EY, Xia M, Liang O, Cheah L, Teplow DB, Xie YH (2018) Surface enhanced Raman spectroscopy distinguishes amyloid Beta-protein isoforms and conformational states. *Protein Sci* 27(8):1427–1438. <https://doi.org/10.1002/pro.3434>
- Zhou Y, Zhang H, Liu L, Li C, Chang Z, Zhu X, Ye B, Xu M (2016) Fabrication of an antibody-aptamer sandwich assay for electrochemical evaluation of levels of beta-amyloid oligomers. *Sci Rep* 6:35186. <https://doi.org/10.1038/srep35186>
- Han X, Man Z, Xu S, Cong L, Wang Y, Wang X, Du Y, Zhang Q, Tang S, Liu Z, Li W (2019) A gold nanocluster chemical tongue sensor array for Alzheimer's disease diagnosis. *Colloids Surf B: Biointerfaces* 173:478–485. <https://doi.org/10.1016/j.colsurfb.2018.10.020>
- Haes AJ, Hall WP, Chang L, Klein WL, Van Duyne RP (2004) A localized surface plasmon resonance biosensor: first steps toward an assay for Alzheimer's disease. *Nano Lett* 4(6):1029–1034. <https://doi.org/10.1021/nl049670j>
- Hu T, Chen C, Huang G, Yang X (2016) Antibody modified-silver nanoparticles for colorimetric immuno sensing of $A\beta_{(1-40/1-42)}$ based on the interaction between β -amyloid and Cu^{2+} . *Sensors Actuators B Chem* 234:63–69. <https://doi.org/10.1016/j.snb.2016.04.159>
- Rahi A, Sattarahmady N, Heli H (2015) Zepto-molar electrochemical detection of Brucella genome based on gold nanoribbons covered by gold nanoblossoms. *Sci Rep* 5:18060
- Negahdary M, Behjati-Ardakani M, Sattarahmady N, Yadegari H, Heli H (2017) Electrochemical aptasensing of human cardiac troponin I based on an array of gold nanodumbbells-applied to early detection of myocardial infarction. *Sensors Actuators B Chem* 252: 62–71. <https://doi.org/10.1016/j.snb.2017.05.149>
- Tondro GH, Dehdari Vais R, Sattarahmady N (2018) An optical genosensor for enterococcus faecalis using conjugated gold nanoparticles-rRNA oligonucleotide. *Sensors Actuators B Chem* 263:36–42. <https://doi.org/10.1016/j.snb.2018.02.097>
- Altintas Z (ed) (2017) Biosensors and nanotechnology: applications in health care diagnostics. Wiley, Hoboken, NJ
- Hayat A, Marty JL (2014) Aptamer based electrochemical sensors for emerging environmental pollutants. *Front Chem* 2:41
- Rozenblum GT, Lopez VG, Vitullo AD, Radrizzani M (2016) Aptamers: current challenges and future prospects. *Expert Opin Drug Discovery* 11(2):127–135
- Zhang Q, Lu Y, Li S, Wu J, Liu Q (2018) Peptide-based biosensors. In: Koutsopoulos S. Peptide applications in biomedicine, biotechnology and bioengineering, 1st edn. Elsevier, pp 565–601
- Dehdari Vais R, Sattarahmady N, Heli H (2016) Green electrodeposition of gold nanostructures by diverse size, shape, and electrochemical activity. *Gold Bull* 49(3–4):95–102
- Sattarahmady N, Firoozabadi V, Nazari-Vanani R, Azarpira N (2018) Investigation of amyloid formation inhibition of chemically and biogenically from Citrus aurantium L. blossoms and Rose damascena oils of gold nanoparticles: toxicity evaluation in rat pheochromocytoma PC12 cells. *Int J Biol Macromol* 112:703–711
- Rahimi-Moghaddam F, Azarpira N, Sattarahmady N (2018) Evaluation of a nanocomposite of PEG-curcumin-gold nanoparticles as a near-infrared photothermal agent: an in vitro and animal model investigation. *Lasers Med Sci* 33(8):1769–1779. <https://doi.org/10.1007/s10103-018-2538-1>
- Sattarahmady N, Heidari M, Zare T, Lotfi M, Heli H (2016) Zinc-nickel ferrite nanoparticles as a contrast agent in magnetic resonance imaging. *Appl Magn Reson* 47(8):925–935. <https://doi.org/10.1007/s00723-016-0801-9>
- Rushworth JV, Ahmed A, Griffiths HH, Pollock NM, Hooper NM, Millner PA (2014) A label-free electrical impedimetric biosensor for the specific detection of Alzheimer's amyloid-beta oligomers. *Biosens Bioelectron* 56:83–90. <https://doi.org/10.1016/j.bios.2013.12.036>
- Wang J, Duan G, Li Y, Liu G, Dai Z, Zhang H, Cai W (2013) An invisible template method toward gold regular arrays of nanoflowers by electrodeposition. *Langmuir* 29(11):3512–3517. <https://doi.org/10.1021/la400433z>
- Kumar A, Mandal S, Selvakannan PR, Pasricha R, Mandale AB, Sastry M (2003) Investigation into the interaction between surface-bound alkylamines and gold nanoparticles. *Langmuir* 19(15):6277–6282. <https://doi.org/10.1021/la034209c>

24. Ross RD, Roeder RK (2011) Binding affinity of surface functionalized gold nanoparticles to hydroxyapatite. *J Biomed Mater Res A* 99A(1):58–66. <https://doi.org/10.1002/jbm.a.33165>
25. Kozłowski LP (2016) IPC - Isoelectric Point Calculator. *Biol Direct* 11:55. <http://isoelectric.org/calculate.php>. Accessed 02 Oct 2019
26. Innovagen AB (2015) *PepCalc.com* - Peptide property calculator. <https://pepcalc.com>. Accessed 02 Oct 2019
27. GenScript (2002) Peptide Molecular Weight Calculator. <https://www.genscript.com/tools/peptide-property-calculator>. Accessed 02 Oct 2019
28. Kang Y, Feng K-J, Chen J-W, Jiang J-H, Shen G-L, Yu R-Q (2008) Electrochemical detection of thrombin by sandwich approach using antibody and aptamer. *Bioelectrochemistry* 73(1):76–81. <https://doi.org/10.1016/j.bioelechem.2008.04.024>
29. Huang Y, Nie X-M, Gan S-L, Jiang J-H, Shen G-L, Yu R-Q (2008) Electrochemical immunosensor of platelet-derived growth factor with aptamer-primed polymerase amplification. *Anal Biochem* 382(1):16–22. <https://doi.org/10.1016/j.ab.2008.07.008>
30. Li L, Zhao H, Chen Z, Mu X, Guo L (2010) Aptamer-based electrochemical approach to the detection of thrombin by modification of gold nanoparticles. *Anal Bioanal Chem* 398(1):563–570. <https://doi.org/10.1007/s00216-010-3922-2>
31. Rahi A, Sattarahmady N, Heli H (2016) Label-free electrochemical aptasensing of the human prostate-specific antigen using gold nanoparticles. *Talanta* 156-157:218–224. <https://doi.org/10.1016/j.talanta.2016.05.029>
32. Hortschansky P, Schroeckh V, Christopeit T, Zandomenighi G, Fändrich M (2005) The aggregation kinetics of Alzheimer's β -amyloid peptide is controlled by stochastic nucleation. *Protein Sci* 14(7):1753–1759. <https://doi.org/10.1110/ps.041266605>
33. Zecca C, Tortelli R, Panza F, Arcuti S, Piccininni M, Capozzo R, Barulli MR, Barone R, Cardinali R, Abbrescia D (2018) Plasma β -amyloid1–42 reference values in cognitively normal subjects. *J Neurol Sci* 391:120–126
34. Pesaresi M, Lovati C, Bertora P, Mailland E, Galimberti D, Scarpini E, Quadri P, Forloni G, Mariani C (2006) Plasma levels of beta-amyloid (1–42) in Alzheimer's disease and mild cognitive impairment. *Neurobiol Aging* 27(6):904–905
35. Andreasen N, Hesse C, Davidsson P, Minthon L, Wallin A, Winblad B, Vanderstichele H, Vanmechelen E, Blennow K (1999) Cerebrospinal fluid β -amyloid (1–42) in Alzheimer disease: differences between early- and late-onset Alzheimer disease and stability during the course of disease. *Arch Neurol* 56(6):673–680

Publisher's note Springer Nature remains neutral with regard to jurisdictional claims in published maps and institutional affiliations.